

Numerical Simulation of Operational-Shock in small form factor drives

P. Bhargava and D. B. Bogy
Computer Mechanics Laboratory
Department of Mechanical Engineering
University of California
Berkeley, CA 94720

Abstract

As non-traditional applications of hard disk drives emerge, their mechanical robustness during the operating state is of greater concern. Over the past few years, there has been an increasing application of small form factor (1" and smaller) hard disk drives in portable consumer appliances and gadgets. A procedure for simulating the operational shock response of a disk-suspension-slider air bearing system is proposed in this paper. A coupled structural-fluid model is presented which can be used to obtain the dynamic response of the slider-suspension-disk system. A commercial program, ANSYS, is used for the finite element models of the suspension and the disk, while the CML dynamic air bearing code is used to concurrently solve the air bearing equations of the system. We obtain not only the responses of the structural components, but also the responses of the air bearing slider. The procedure is convenient for practical application as well as being highly accurate, since it implicitly solves the structural and air bearing problems simultaneously. It is used to simulate the shock response of a 1" drive. The air bearing has different responses for upward and downward shocks (which are referred to as positive and negative shocks, respectively). For negative shocks, slider-asperity contacts are observed to occur when a strong shock is applied. For positive shocks, we observe a collapse of the air bearing when the shock is sufficiently strong, which is followed by severe contacts between the slider and the disk due to the 'head-slap' phenomenon.

1 Introduction

The interest in the effects of shock on hard disk drives has come into currency due to the increasingly hostile environments encountered in the usage of the portable computer as well as the application of hard disk drives in consumer devices such as MP3 players and PDAs. As non-traditional applications of hard disk drives emerge, their mechanical robustness under shock and other mechanical disturbances during different states are of greater concern. Normal drives cannot properly function in these kinds of environments. The main effects of shock are malfunctions during the operating state, damage during initial assembly, testing, installation, and all unfavorable situations caused by the final users.

As stated by Zeng and Bogy [1], there are essentially three approaches for dealing with the shock problems. The first approach is to design and install a suitable isolation system for the disk drives. The second is to design a robust servo control mechanism to prevent read/write errors during the shock. The third is to design a robust mechanical system and slider/disk interface that is resistant to shock. Our research focuses on the third approach.

There have been various experimental and simulation studies [1-9] on the shock response of the mechanical system and its effects on the head/disk interface. However, much of the published works have been limited to the non-operating state of the drives, and/or to the component level. As the fly heights (FH) continue to reduce and more and stronger disturbances during the operating state are encountered, especially with the emergence of small form factor drives for consumer electronics, a better understanding of the effects of these disturbances on the head/disk interface is essential. Various published papers [1-5] considered shock simulation of disk drives in the operating state. They used quite different approaches.

Jiang et al. [5] focused on the rotating disk in their paper. The suspension and slider were modeled as a spring-mass system, and the air bearing was modeled as another spring. The

shock was specified at the end of the suspension and on the disk hub. The solution was obtained by using the multi-modal expansion approximation, applying the Galerkin method to the resulting equations, and using the Newmark β method to solve the final equations. The air bearing responses, i.e., the dynamic FH, was obtained from the deformation of the spring that models the air bearing. Their method is expected to model the disk response very well. However, it does not provide sufficient insight into the response of the arm-suspension and the air bearing.

Harrison and Mundt [6], on the other hand, focused on the air bearing. The suspension and slider were modeled as a lumped multiple DOF spring-mass system. The air bearing was modeled by the usual Reynolds equation, and it was solved numerically. They measured the disk's response at the point under the slider and the arm's response at the end of the arm. Then they used this measured data as input into the air bearing simulation code, and they obtained the dynamic FH. It is inconvenient to apply their method because it requires the measurement data for each case of interest. Furthermore, they did not describe the procedure to obtain the lumped spring-mass model of the arm-suspension, and they did not show the effect of this simplification on the results.

Jayson et al [2, 3] developed a finite element model of a hard disk drive to investigate the transient response of an operational drive subject to shock and vibration. The air bearing stiffness of the head disk interface was determined from a finite element solution of the Reynolds equation and approximated with linear springs. They analyzed the structural response for several types of sliders with a wide range of air bearing stiffness. Because of the approximate modeling of the air bearing using linear springs, they were not able to capture the true behavior of the air bearing.

Zeng and Bogy [1] proposed a method whereby they separate the simulation work into two essentially uncoupled sets. They developed a finite element model of the disk and suspension system and used it to obtain the dynamic normal load and moments applied to the slider air bearing. These were then used as input data for an air bearing dynamic

simulator to calculate the dynamic flying attitudes. This procedure was later also used by Jayson et al [4]. They were able to obtain not only the responses of the structural components, but also the responses of the slider air bearings. The results from this method were reasonably accurate; however the assumption that the two sets of simulations are uncoupled can lead to some inaccuracies in the simulations. Also, simulations where the air bearing exhibits highly nonlinear behavior, such as when the air bearing collapses, may require iterations between the structural and air bearing simulations, thereby making the process cumbersome and computationally more expensive.

Therefore, more research is required for shock simulation of the disk drives and slider air bearings during the operating state. In this paper we propose a procedure for simulating the shock response of a disk-suspension-slider air bearing system simultaneously.

Simulations were done using the new CML Shock simulator, which uses ANSYS to do the structural modeling of the suspension. The simulations were carried out for the Femco slider from a commercially available 1” drive (figure 1) with a particular suspension (figure 2). Shocks were modeled as acceleration pulses to the structural system (figure 3). The pulse width was kept fixed at 0.5 ms and the magnitude of the shock pulse was varied from -800 G to 600 G.

2 Simulation procedure

2.1 Suspension and Disk response to shock

To better understand shock effects we need to know the shock responses of both structural components. In this section we will look at the behavior of the suspension and the disk in the event of a shock. A finite element model of the suspension-disk system was used to study the dynamic behavior of the suspension and the disk during shock.

2.1.1 Disk response

The excitation of the shock is symmetric about the rotation axis of the disk. It is well known that a rotating disk has three types of modes. The first type is the symmetric modes with m nodal circles and no nodal diameters ($m, 0$), which have frequencies that only slightly increase with the rotating speed, which is due to centrifugal stiffening. These are also referred to as the ‘umbrella’ modes of vibration (figure 4a). Their frequencies and mode shapes are very similar in the operating and non-operating states. The second is the asymmetric modes with zero nodal circles and n nodal diameters ($0, n$), each of which splits into two modes in the operating state (figure 4b). They have no response to symmetric excitations. The third is the coupled asymmetric modes (m, n) ($m > 0, n > 0$) (figure 4c), which are higher frequency modes, and their responses are much smaller than the responses from the low frequency modes for ordinary shocks (e.g., 0.5 ms half sinusoidal acceleration). A finite element model for the disk was created in ANSYS using shell elements. The disk was subject to a 200 G shock for two cases: when the disk was rotating at 3600 RPM and in the stationary state. Figure 5 shows the z -displacement of a point on the outer periphery (OD) of the disk for both cases. Figure 6 shows the frequency spectra of the displacement. The first peak corresponds to the first umbrella mode of vibration of the disk. The other small peaks correspond to radial modes of vibrations of the disk, but the power contained within these is relatively very small. Thus we can see that since the disk response is predominantly axisymmetric, we can assume there is no significant difference in the shock responses of the disk during the operating and non-operating states when the shock is applied axially to the hub. In addition, the change in frequency due to the spinning of the disk is also negligible. Although the slider’s load on the disk is not axisymmetric, it has been shown previously that its contribution to the disk response is negligible [1]. Therefore, the disk responses to a symmetric shock are expected to be mainly from the axisymmetric modes, and they are similar in the operating and non-operating states. Hence, it is expected that this

assumption will not cause a significant error in the simulation results. For non-axial shocks it will be important to consider the rotation of the disk while simulating shock.

2.1.2 Suspension Response

FE shock simulations were also carried out for the suspension. Figure 7a shows the z-displacement for the slider centre on the suspension as well as plots for the pitch and the roll during a shock of 200 G. Figure 7b plots the frequency spectra for the same. The first peak is observed at 300 Hz which corresponds to the first bending mode of the suspension. We see that most of the power in the z-displacement is contained in this mode. For pitch (figure 7c and 7d), we see that most of the energy is contained in this mode as well as modes around 2000 Hz, which correspond to the second bending mode of the suspension and bending modes of the flexure. For roll, (figures 7e and 7f), we see that most of the energy is contained at 500 Hz and 3000 Hz which correspond to torsion modes of the suspension and the flexure.

2.2 Shock simulator

The main shock simulator consists of two modules: one for structural modeling and another for the air bearing calculations.

2.2.1 Air bearing program

The program used to perform air bearing calculations is a modification of the CML dynamic air bearing simulator [10]. The air bearing program uses a 6-DOF model, three of which are used to model the slider attitude and the other three to model the disk orientation. The three degrees of freedom for the slider represent the fly-height, the pitch and the roll of the slider.

During the event of a shock, the disk behavior also becomes very important. To include the effects of the disk dynamics on the air bearing, we use a three parameter model to represent the disk. It is assumed that the area of the disk under the slider behaves as a

plane. This assumption is valid since the wavelengths of the modes of the disk are much larger than the dimensions of the slider. The area of the disk under the slider can hence be characterized by three parameters: namely the z-height, the ‘pitch’ or the angle the plane of the disk area makes with the y-axis, and the ‘roll’ or the plane angle in along the x-axis (see figure 8). Figure 9 shows the variation of these three parameters for a typical shock. We see that the variation in the ‘roll’ angle for the disk is much greater than the ‘pitch’. This is because the primary mode of vibration of the disk is the ‘umbrella’ mode, which would correspond to a change in the ‘roll’ angle of the plane.

2.2.2 Structural modeling

The structural behavior of the suspension is modeled in ANSYS, which is a commercial finite element modeling program. A script was written for ANSYS using APDL (ANSYS programming language) to interface with the air bearing program and run analyses on the suspension model.

2.2.3 Coupling scheme

The basic structure of the program is shown in the flowchart in figure 10. At each time step, say t_{n+1} , we need to calculate the air bearing/contact forces acting on the slider, f_{n+1} , and the displacements of the slider, d_{n+1} (i.e. z-displacement of the slider centre, the pitch and the roll angles). This coupling between the air bearing and the structural dynamics of the suspension is solved simultaneously. The solution scheme is shown in the flowchart in figure 10. The air bearing simulator calculates the forces at time t_{n+1} using its current guess for the displacements at time t_{n+1} , which is initially the displacements at time t_n . These values of forces are sent to ANSYS (which is running a dynamic structural analysis of the suspension) which applies these at time t_{n+1} to calculate the displacements at time t_{n+1} . These displacements are read by the air bearing simulator which calculates the error in its current guess of the displacement with respect to the new guess of displacements obtained from ANSYS. If the error is less than a tolerance value the

simulation proceeds to the next time step, otherwise it recalculates the values of the air bearing forces at t_{n+1} using the updated displacement guess and passes them to ANSYS, which performs the load step for t_{n+1} again. This process is repeated until convergence is achieved. Though the contractive nature of the air bearing-structural coupling has not been verified, this scheme is found to always converge in practice.

3 Results

Simulations were run using different magnitudes of shock in the + and - z directions. This section presents the results. A positive shock is defined as an acceleration impulse in the positive z direction (with the axes defined as shown in figure 11). Similarly a negative shock is one in the negative z direction. It is interesting to note that inside a multi-head disk drive, heads on opposite sides of a platter will experience positive and negative shocks for any given shock event.

We define ‘absolute’ and ‘relative’ quantities of interest to help us analyze our results. The absolute quantities for the slider, i.e. the absolute displacement, pitch and the roll are defined as the absolute displacements and angles measured with respect to the disk surface in the undeformed configuration. Similarly because of the manner in which we have parameterized the disk surface, we can define similar quantities for the disk.

The relative quantities are defined as the difference between the absolute quantities for the disk and the slider. In essence these would define the relative displacement between the disk and the slider, and the relative angles between the two for the pitch and the roll. These are the quantities of interest for characterizing the air bearing behavior.

3.1 Negative shock

Negative shocks are shocks in the negative z direction.

Figure 12 shows the response for a simulation of a negative shock of 200 G. We plot the absolute displacements at the slider centre for the slider and the disk followed by the

relative displacement. We see that during the event of a negative shock both the disk and the suspension move down, but the suspension being more flexible than the disk has a tendency to displace more, which causes the air bearing to develop a compressive force. The third plot shows the variation of the z displacements at the TEC. The trend in the relative nominal FH shown in the fourth plot is opposite to that of the displacements at the slider centre primarily due to the change in pitch of the slider. In the sixth plot, we see that the relative pitch also decreases during the shock. A point to note here is that since the response of the disk is primarily axisymmetric, the pitch motion of the disk depends primarily on the skew angle. If the skew angle had been positive, we would have observed different pitch behavior. The final pair of plots show the variation of the roll angle during the shock. The absolute roll response of the system is much stronger than the pitch response of the system because the umbrella mode of the disk contributes more strongly to the roll displacement. Figure 13 (top) plots the air bearing and the contact forces during the shock event. The air bearing develops an increased positive air bearing force to balance the increased gram load caused by the suspension pushing into the disk. We observe that the variation in the negative (suction) force is small compared to the variation in positive pressure force. The next plot (bottom) shows the variation of the impact force and the asperity contact force during the shock. Asperity contact force is the contact force calculated quasi-statically using the Greenwood-Williamson contact model, whereas the impact force is the dynamic force caused by the slider hitting the disk. The asperity contact force is calculated when any point on the slider has a flyheight that is below the glide height, whereas the impact force is generated when the fly height of any point on the slider becomes negative. We see that there is no impact for moderate values of shock (200 G) and contact forces are generated when part of the slider is flying below the glide height.

Since the air bearing force developed during the shock is compressive, it is observed that the slider is able to follow the disk surface for moderate shock magnitudes, with small modulations in the 'relative' attitudes.

Figure 14 plots the absolute and relative attitude for a shock magnitude of 400 G followed by the air bearing and contact forces in figure 15.

Figures 16 and 17 plot the attitudes and forces for a shock magnitude of 800 G. Here we observe relatively large contact and impact forces, which are however much smaller than those observed for positive shocks (which is discussed in the next section).

In figure 18 we plot the variation of the nominal fly height for various values of the shock magnitude. The slider achieves its maximum nominal fly height during the shock, and the minimum value of the fly height occurs during the ensuing vibrations. Figure 19 plots the variation in the air bearing forces during the shock. The maximum air bearing force develops during the actual shock pulse, whereas the minimum air bearing force is observed during the ensuing vibrations. In figure 20 we plot the quantities of interest which are the contact and the impact forces. Initially we observe an increase in asperity contact forces, which levels off for stronger values of shock. This is expected because the asperity contact forces are calculated quasi-statically, and as they are a function of the minimum flying attitude. We also see that there is no impact between the slider and the disk up until about 400 Gs. However for shocks over 400 G the impact force increases rapidly with the G level. This impact force would be the primary mode of failure during negative shocks. We note that the air bearing is unlikely to break since the negative air bearing force is very small in magnitude. For the slider to pull off the disk and the air bearing to break would require a negative air bearing force of at least a few grams, as we will see in the next section.

3.2 Positive shock

Positive shocks are characterized by an acceleration pulse in the positive z direction. Simulations were run for positive shock with shock amplitudes from 100 G to 600 G. In figure 21 we plot the absolute and relative attitude graphs for a positive shock of 200 G. We see that due to positive shock both the disk and the suspension move up, but the suspension being more flexible than the disk, has a tendency to lift off the disk, which causes the air bearing to develop a negative pressure. It is observed that for low values of shock, the air bearing is able to support the negative load and retain the slider on the disk. The slider is able to follow the vibrations of the disk with small modulations in its relative attitude. Figure 22 plots the air bearing and contact forces during the event of the 200 G shock. The air bearing force achieves a minimum value of -0.5 g, which does not cause the air bearing to break. The minimum fly height goes below the glide height during the shock pulse which causes asperity contact forces to come into play; however we observe that there is no impact.

Increasing the magnitude of the shock to 300 G, we see that during the event of the shock, the air bearing is no longer able to support the negative load, and so it breaks. Figures 23 and 24 plot the absolute and relative attitudes of the system and the air bearing and contact forces for the 300 G shock. From the air bearing force plot (figure 24, top) We see that the air bearing is able to support the slider up to a negative load of about -2 g, after which the air total pressure force falls as the air bearing breaks. However even after the air bearing breaks the slider does not lift off the disk completely. The lifting of the slider off the disk is dependant on the velocity of the slider at the time the air bearing breaks. If the slider is moving up, it will lift off the disk. However if it is on its way down, it will not completely lift off the disk as observed here. During the ensuing vibrations the air bearing is still able to develop a positive force so as to not allow the slider to contact the disk. However the air bearing does not re-establish immediately since we observe

there is no negative pressure force and since the attitude is much higher than the steady state attitude of the slider.

Further increasing the shock to 500 G we see that the air bearing breaks completely and the slider goes flying off the disk into the natural vibration mode of the suspension. Figures 25 and 26 plot the attitudes and forces for 500 G. During the shock the air bearing develops a negative load of almost -3.5 g, which causes the air bearing to break completely. The slider flies off, and after the shock pulse, we observe severe impacts between the disk and the slider. This sort of a shock would likely lead to failure of the drive.

In figure 27 we plot the variation of the maximum and minimum air bearing forces as a function of shock magnitude. The maximum air bearing force is observed in the period after the shock, in the consequent vibrations. However the air bearing breaks during the shock event itself for shock magnitudes greater than 300 G, hence it does not make sense to plot the maximum air bearing force in these cases. The minimum air bearing force is the maximum lift off force generated during the shock. For shocks greater than 300 G, the slider lifts off from the disk. However we see that the liftoff force continues to increase even after 300 G which is due to the rate terms in the Reynolds equation.

Figure 28 plots the contact and impact forces as a function of the shock magnitude. Impact forces are zero up to shocks of about 200 G; however they rise sharply for shocks above 300 G.

4 Conclusion

Shock simulations were run using the new CML Shock simulator with a Femco slider and suspension in a 1" hard disk drive. We simulated shocks in the z direction using a half sinusoid acceleration pulse with a width of 0.5 ms and varying amplitude from -800 G to 600 G.

The disk drive system was found to be extremely robust for shocks with negative magnitudes (referred to as ‘negative shocks’) and much more susceptible to failure during shocks with positive magnitudes (referred to as ‘positive shocks’).

The primary mode of failure for negative shocks was found to be the slider contacting the disk during the shock event itself. The air bearing was found to be able to sustain relatively large compressive loads of up to 7 grams (at 800 G) without failing.

The primary mode of failure for positive shocks was found to be due to contacts between the slider and the disk, caused by the slapping of the slider against the disk in the event of the air bearing breaking. The air bearing was found to fail for negative gram loads beyond -2.3 g (300 G).

References

- [1] Zeng, Q. and Bogy, D. B., 2000, “Numerical Simulation of Shock Response of Disk-Suspension-Slider Air Bearing Systems in Hard Disk Drives”, Technical Report No 2000-003, Computer Mechanics Lab, Department of Mechanical Engineering, University of California, Berkeley.
- [2] Jayson, E.M., Murphy, J., Smith, P.W. and Talke, F.E., 2003, “Effects of Air Bearing Stiffness on a Hard Disk Drive Subject to Shock and Vibration”, *ASME Journal of Tribology*, Vol. 125, pp. 343-350.
- [3] Jayson, E.M., Murphy, J., Smith, P.W. and Talke, F.E., 2002, “Shock and Head Slap Simulations of Operational and Non-operational Hard Disk Drives”, *IEEE Trans. on Magnetics*, Vol. 38, No. 5, pp. 2150-2153.
- [4] Jayson, E.M., Murphy, J., Smith, P.W. and Talke, F.E., 2003, “Shock Modeling of the Head–Media Interface in an Operational Hard Disk Drive”, *IEEE Trans. on Magnetics*, Vol. 39, No. 5, pp. 2429-2432.

- [5] Jiang, Z. W., Takashima, K., and Chonan, S., 1995, "Shock-Proof Design of Head Disk Assembly Subjected to Impulsive Excitation," *JSME International Journal*, Series C, Vol. 38, No. 3, pp. 411-419.
- [6] Harrison, J. C. and Mundt, M. D., 2000, "Flying Height Response to Mechanical Shock During Operation of a Magnetic Hard Disk Drive," *ASME Journal of Tribology*, Vol. 122, No. 1, pp. 260-263.
- [7] Edwards, J. R., 1999, "Finite Element Analysis of the Shock Response and Head Slap Behavior of a Hard Disk Drive," *IEEE Trans. of Magnetics*, Vol. 35, No. 2, pp. 863-867.
- [8] Kumar, S., Khanna, V., and Sri-Jayantha, M., 1994, "A study of the Head Disk Interface Shock Failure," The 6th MMM-Intermag Conference paper.
- [9] Kouhei, T., Yamada, T., Keroba, Y., and Aruga, K., 1995, "A Study of Head-Disk Interface Shock Resistance," *IEEE Trans. on Magnetics*, Vol. 31, No. 6, pp. 3006-3008.
- [10] Ishimaru, N., 1996, "Experimental Studies of a Head/Disk Interface Subjected to Impulse Excitation During Non-operation," *ASME Journal of Tribology*, Vol. 118, pp. 807-812.
- [11] Allen, A. M. and Bogy, D. B., 1996, "Effects of Shock on the Head-Disk Interface," *IEEE Trans. of Magnetics*, Vol. 32, No. 5, pp. 3717-3719.
- [12] Chen, L., Hu, Y. and Bogy, D. B., 1997, "The CML Air Bearing Dynamic Simulator, V4.21", Technical Report No 1998-004, Computer Mechanics Lab, Department of Mechanical Engineering, University of California, Berkeley.

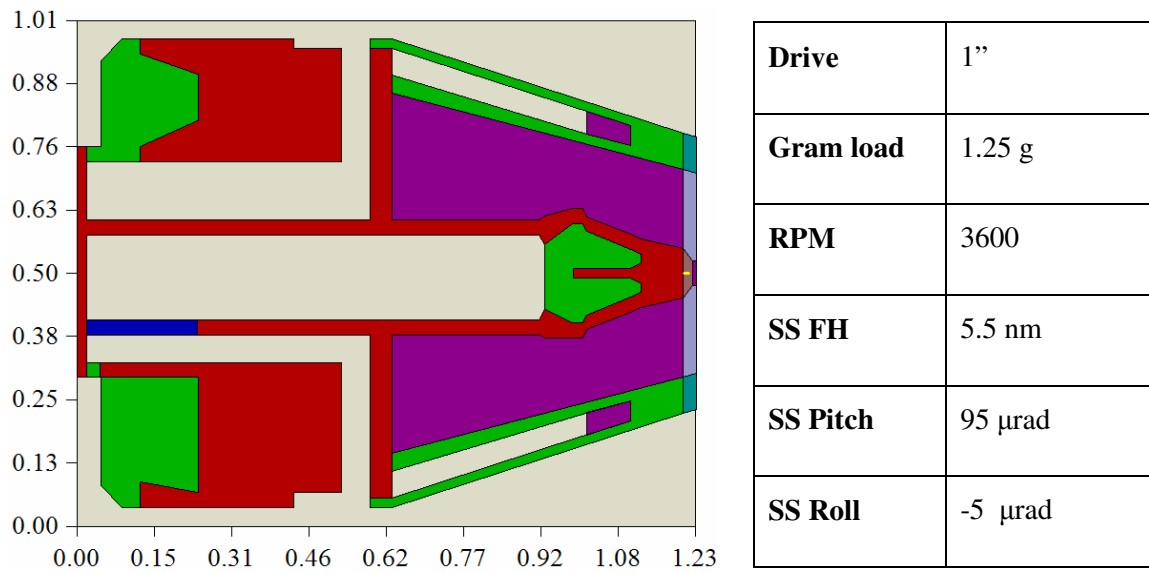


Fig 1. Femco Slider and parameters used for the simulations

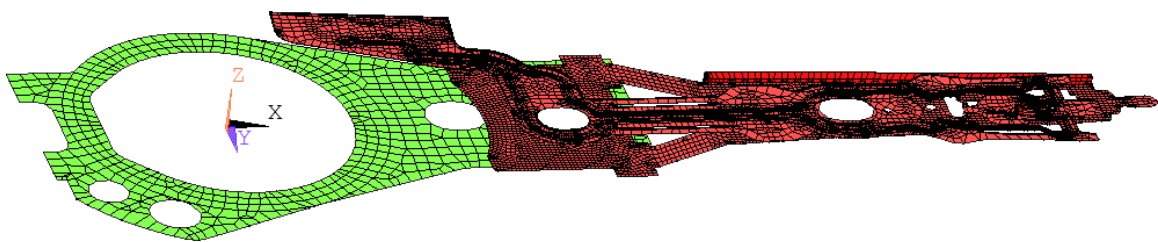


Fig 2. 1" drive suspension

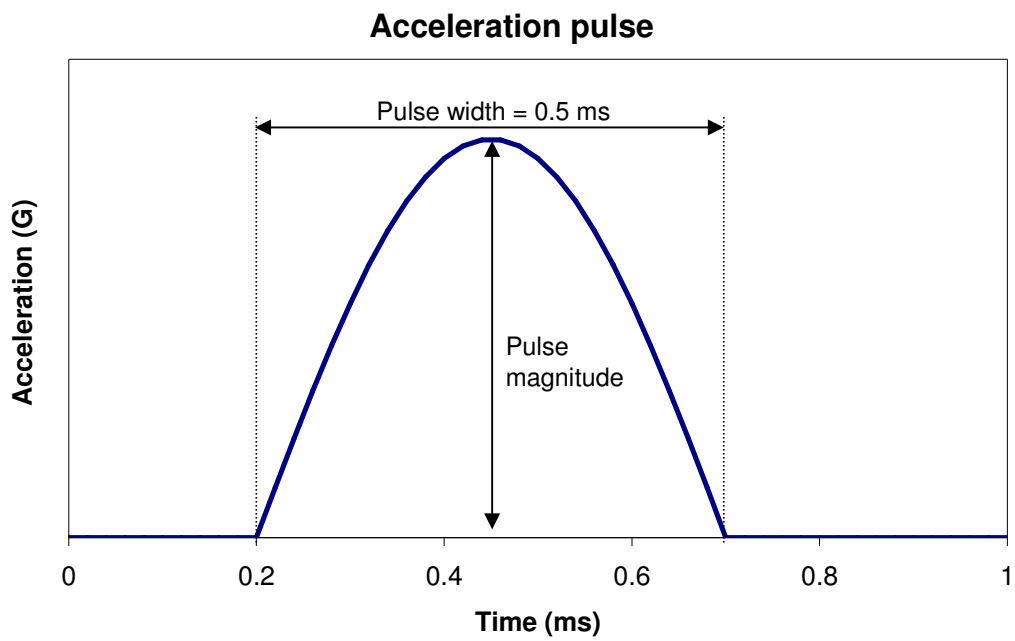


Fig 3. Acceleration pulse

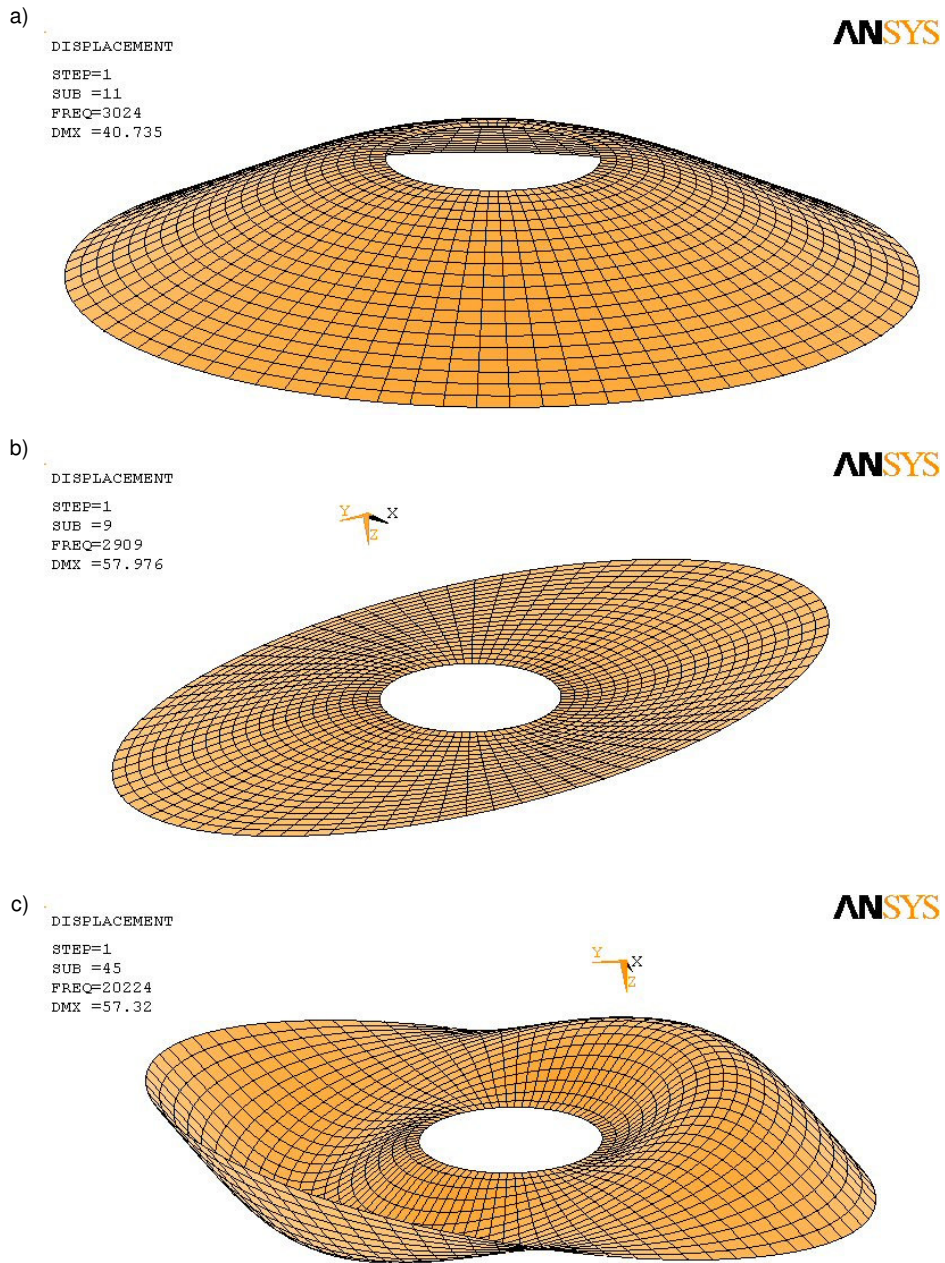


Fig 4. Modes of vibration of the disk: Umbrella mode, radial mode, coupled mode

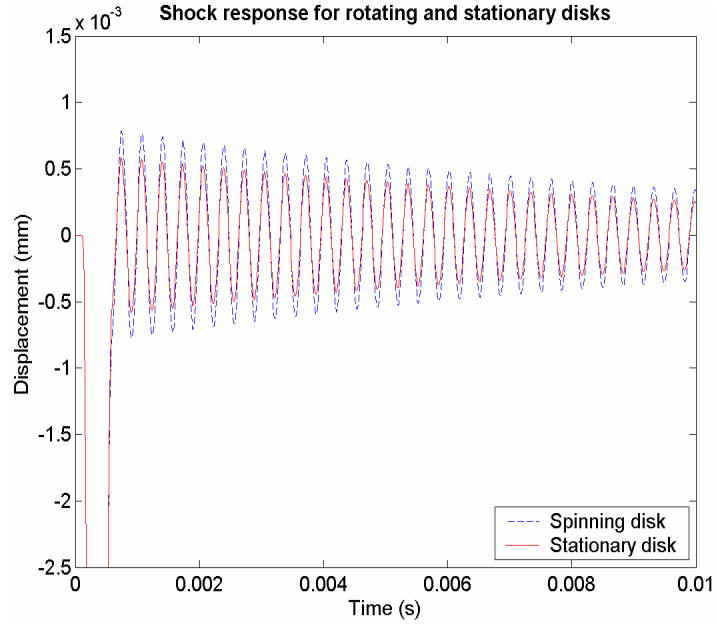


Fig 5. Disk z-response to shock for spinning and stationary disks

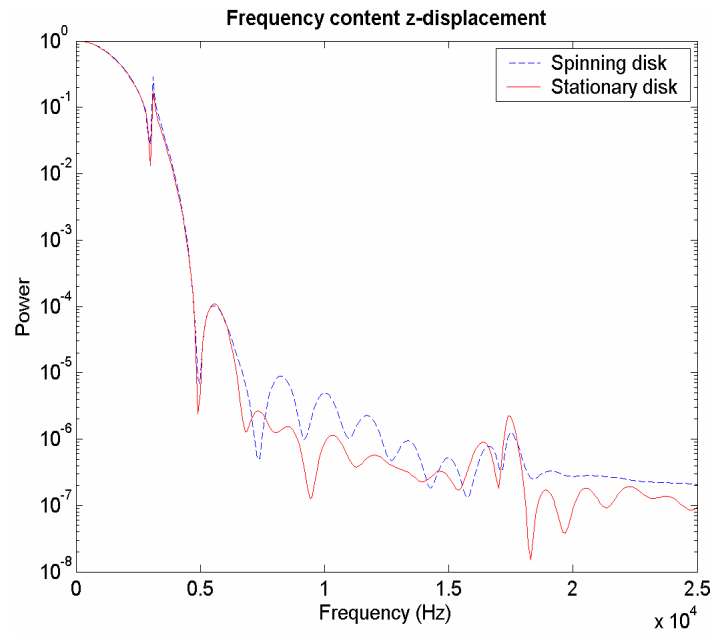


Fig 6. Power spectra of disk z-response for spinning and stationary disks

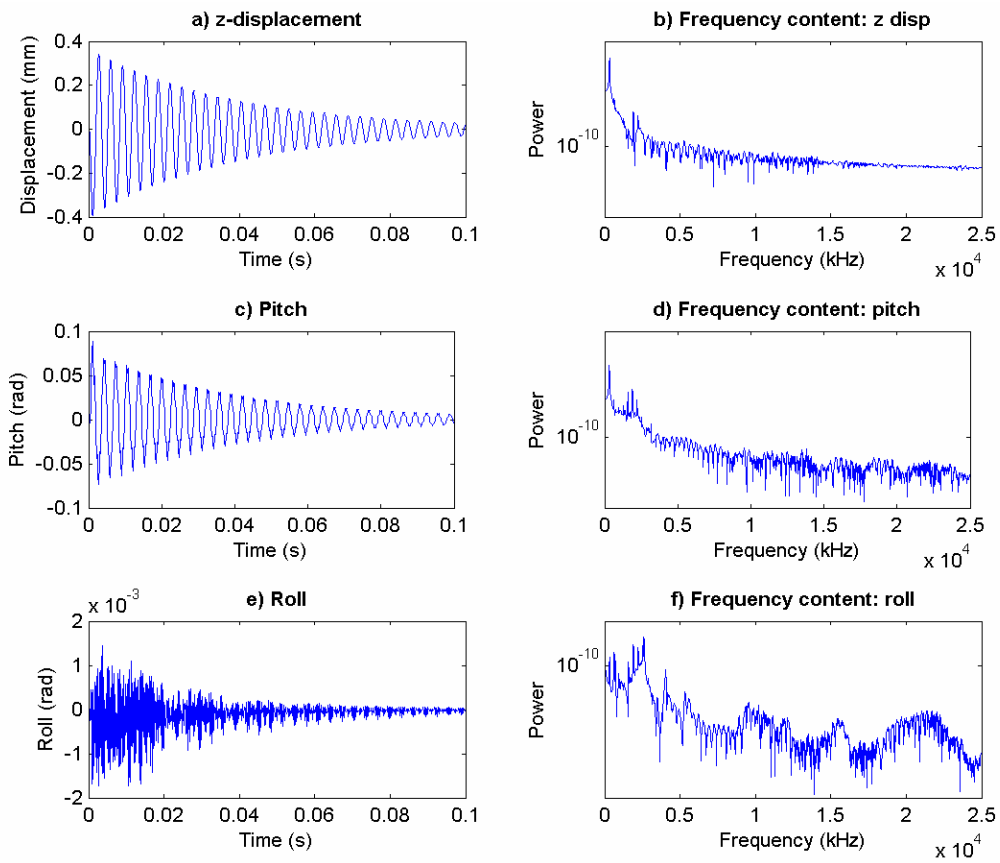


Fig 7. Suspension response to shock and associated power spectra

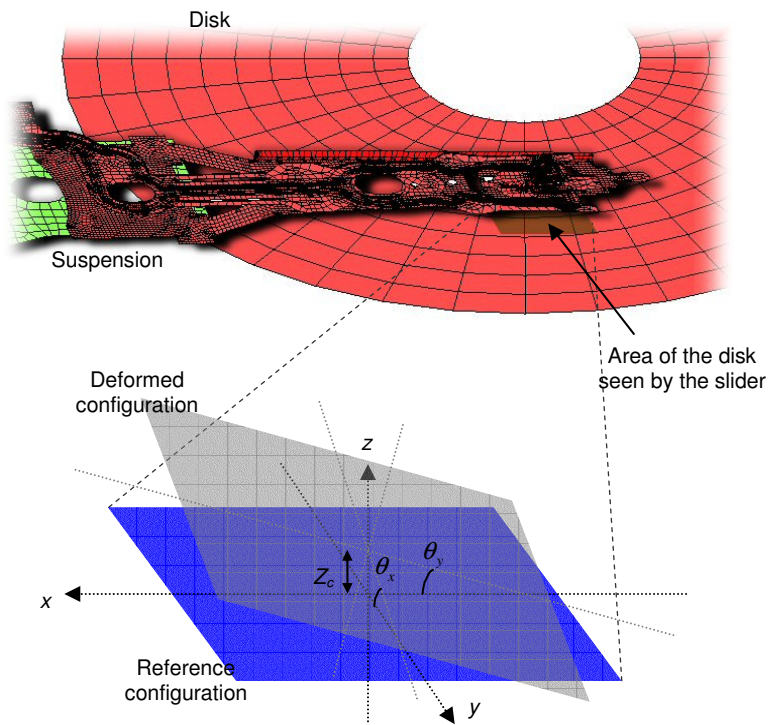


Fig 8. Parameterization of disk behavior

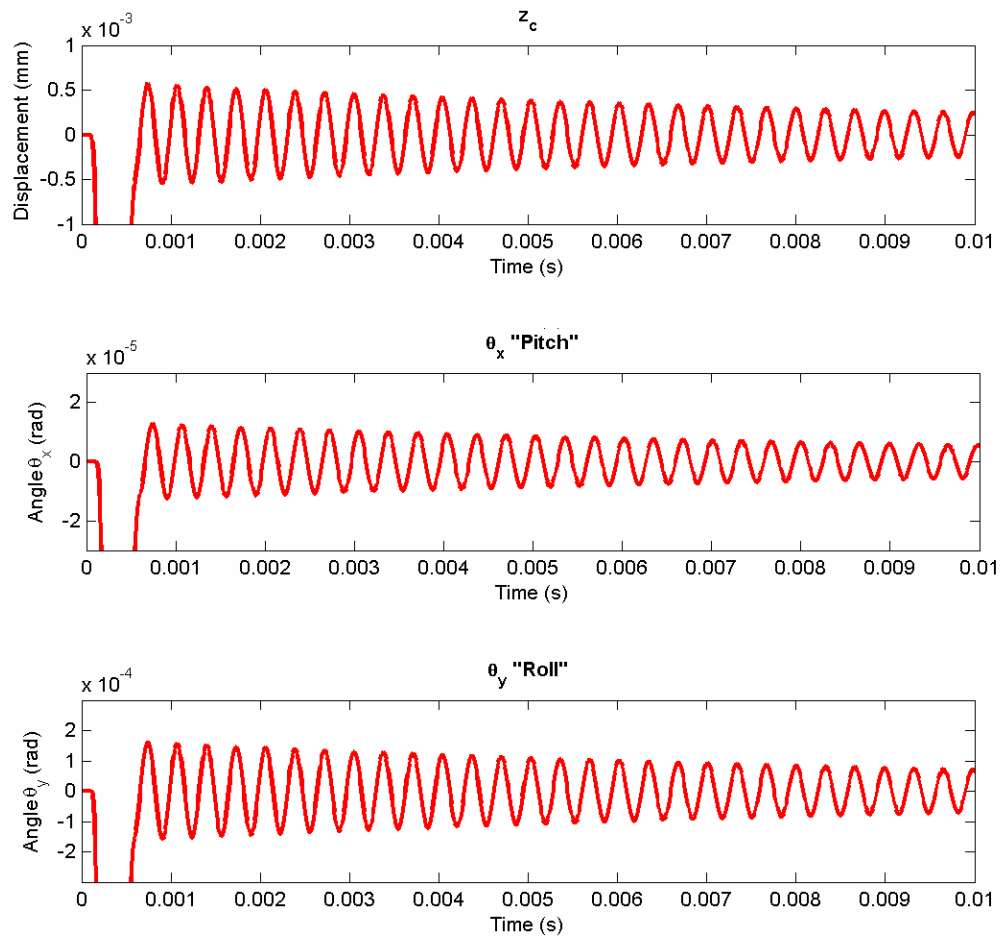


Fig 9. Disk parametric shock response

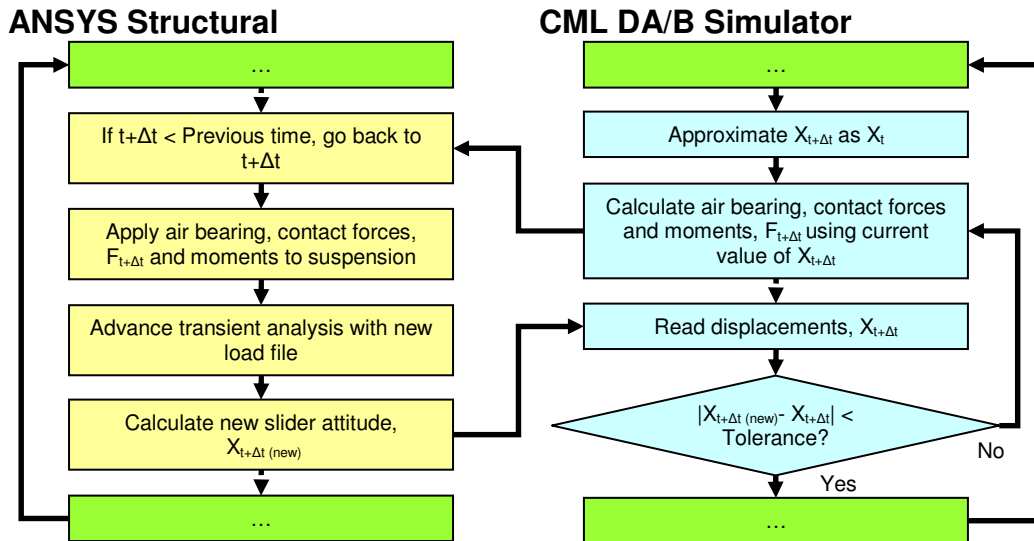


Fig 10. The CML Shock simulator

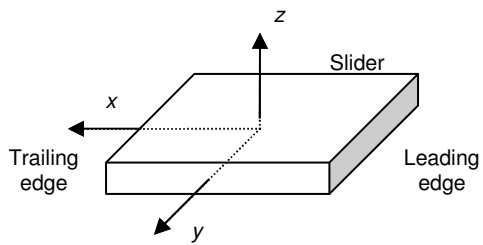


Fig 11. Coordinate system

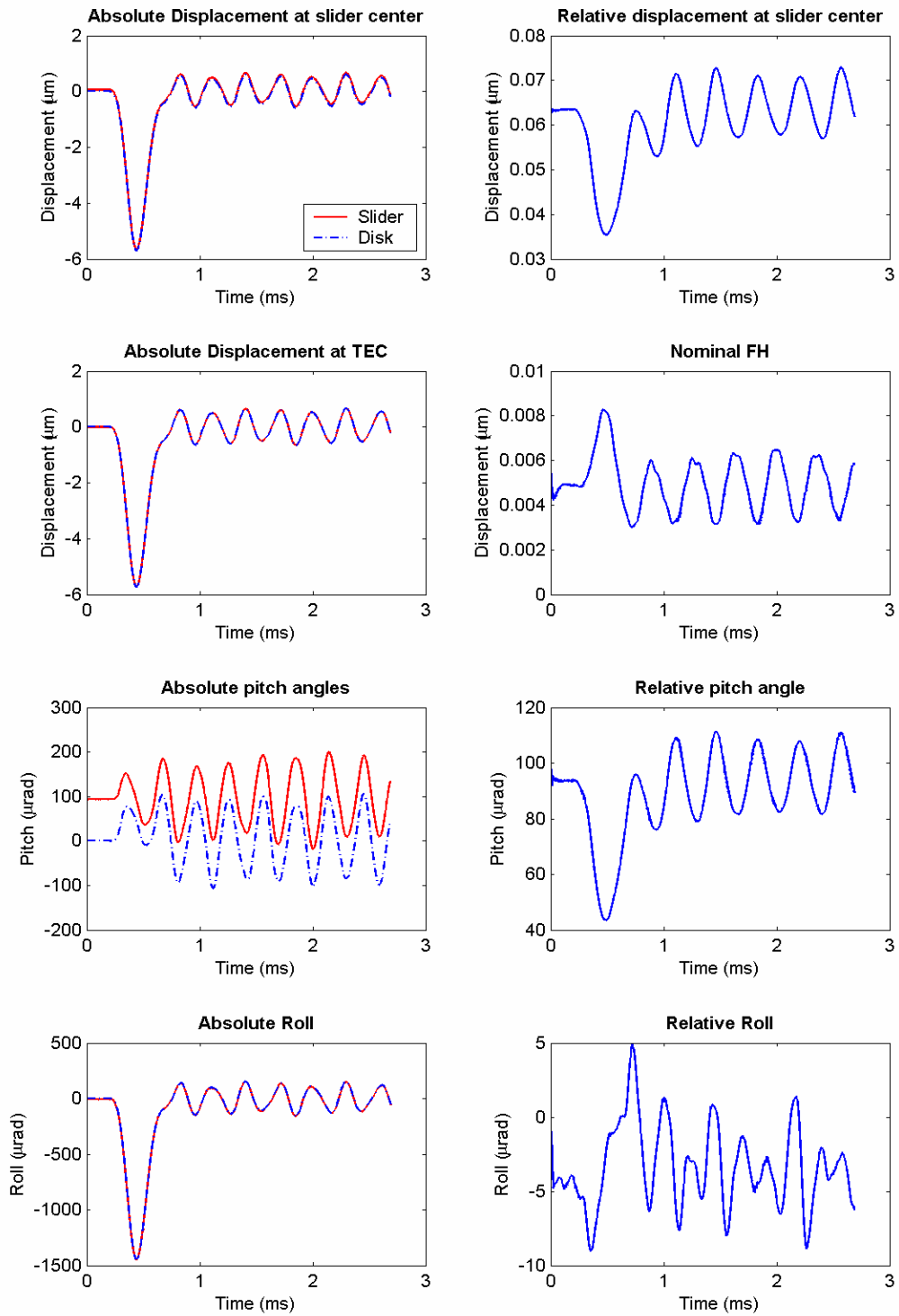


Fig 12. Absolute and relative attitude for negative 200 G shock

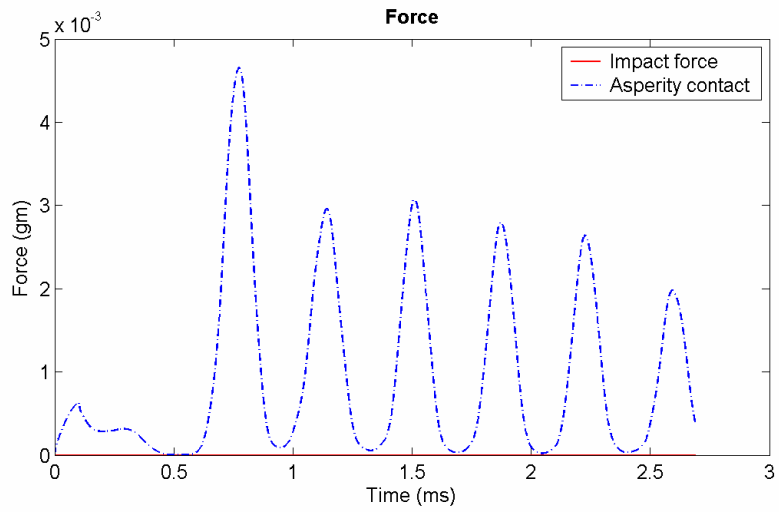
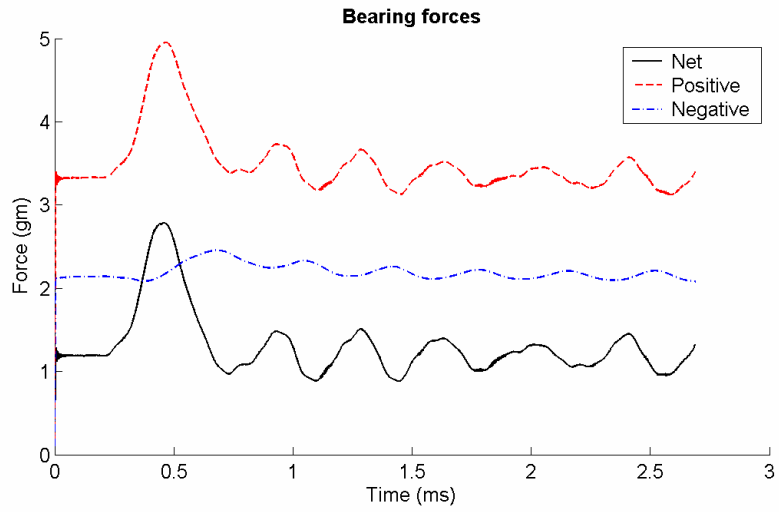


Fig 13. Air bearing and contact forces for negative 200 G shock

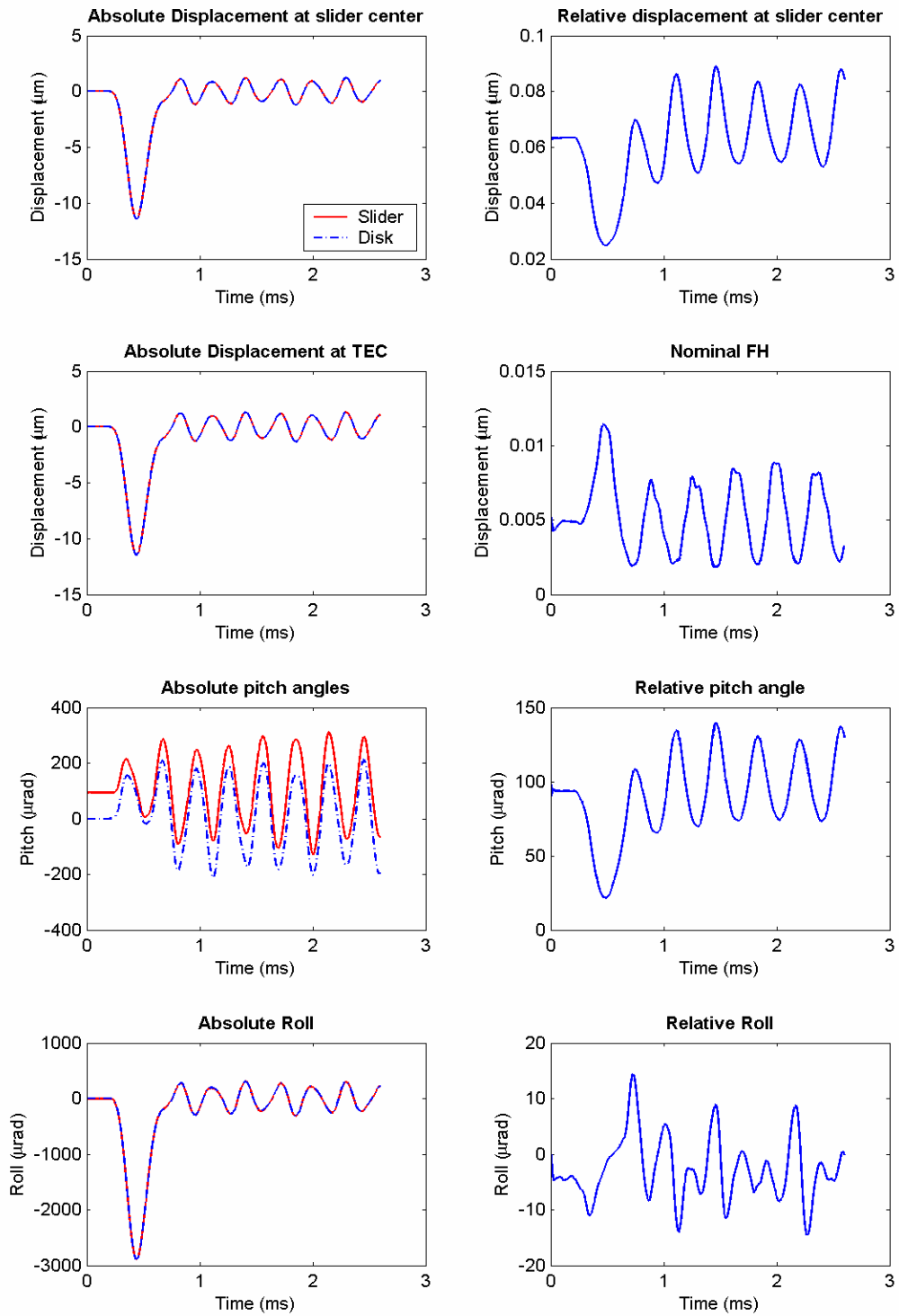


Fig 14. Absolute and relative attitude for negative 400 G shock

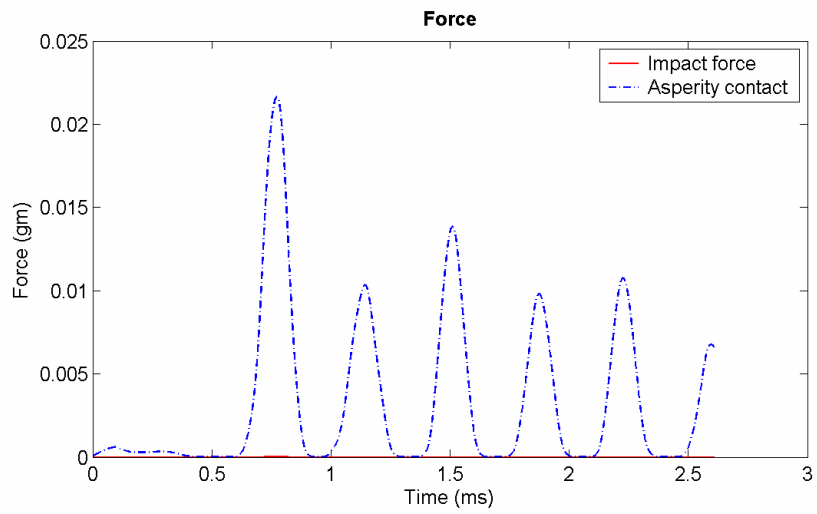
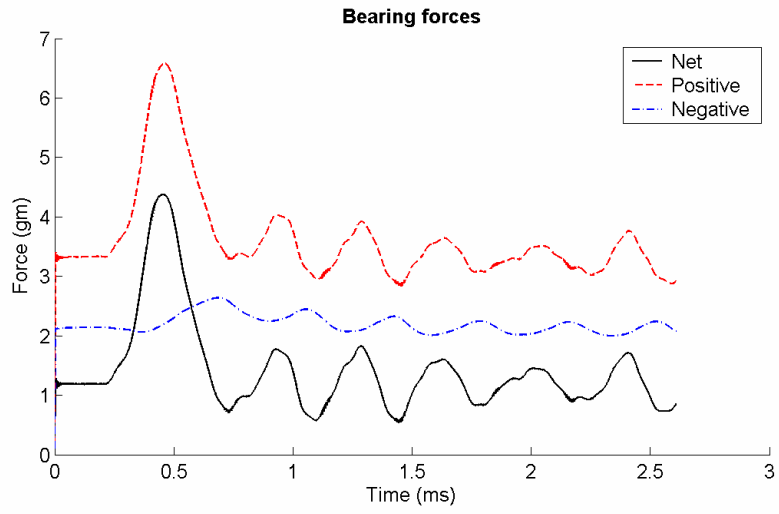


Fig 15. Air bearing and contact forces for negative 400 G shock

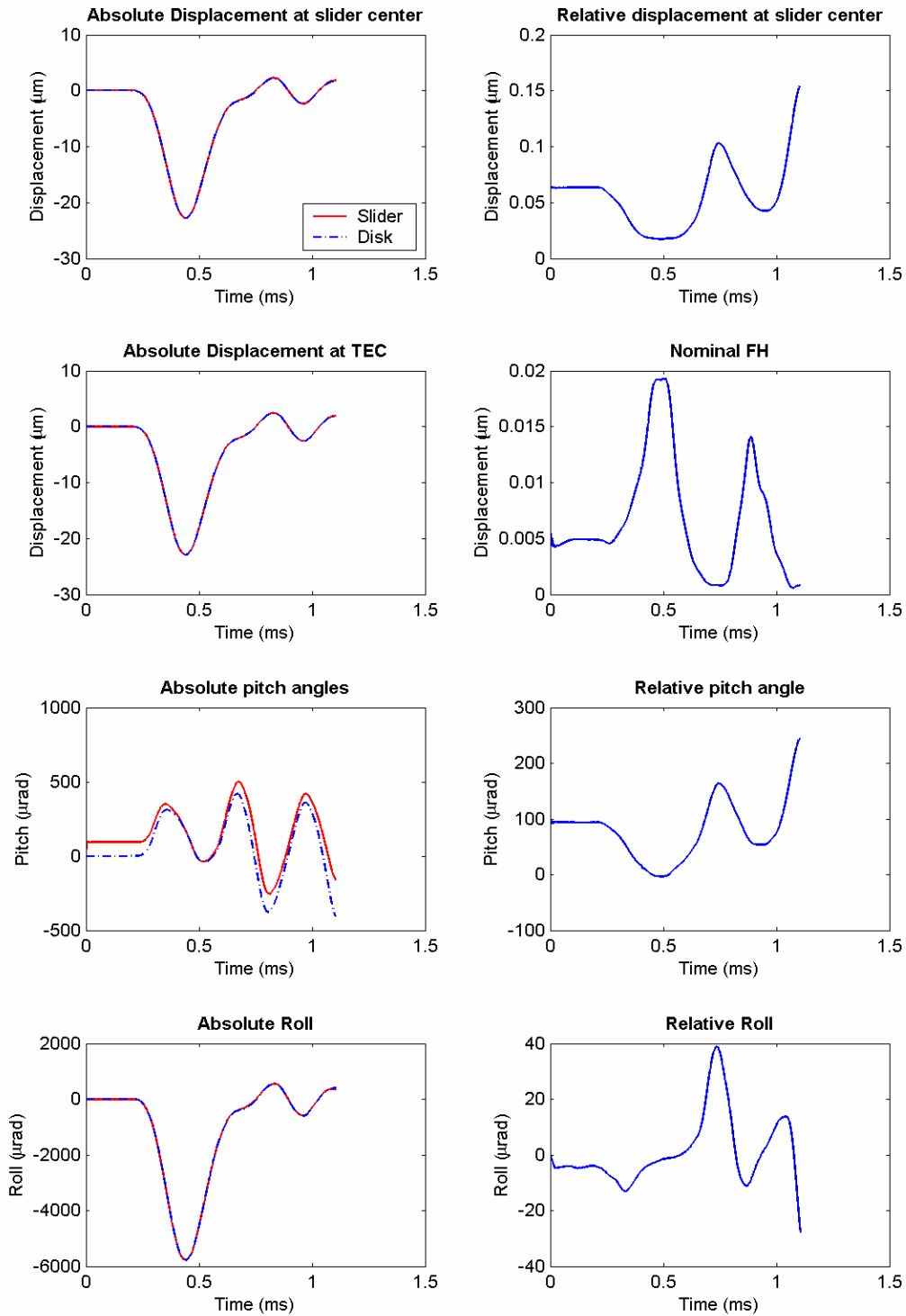


Fig 16. Absolute and relative attitude for negative 800 G shock

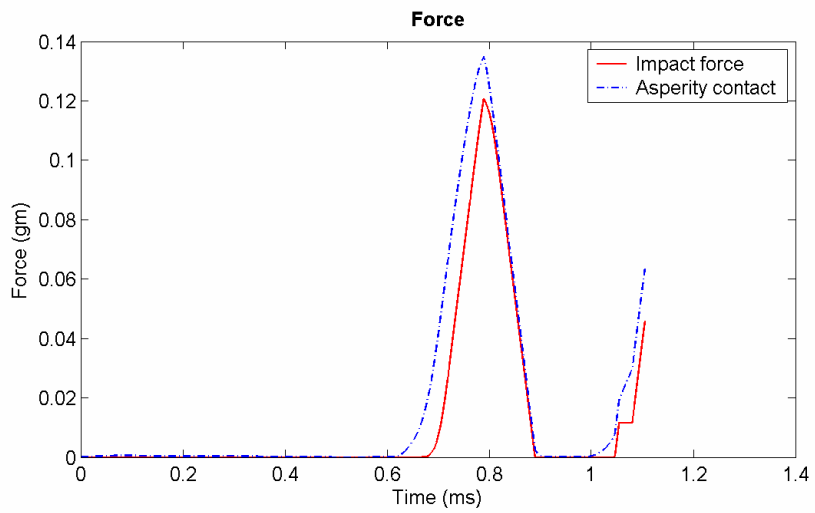
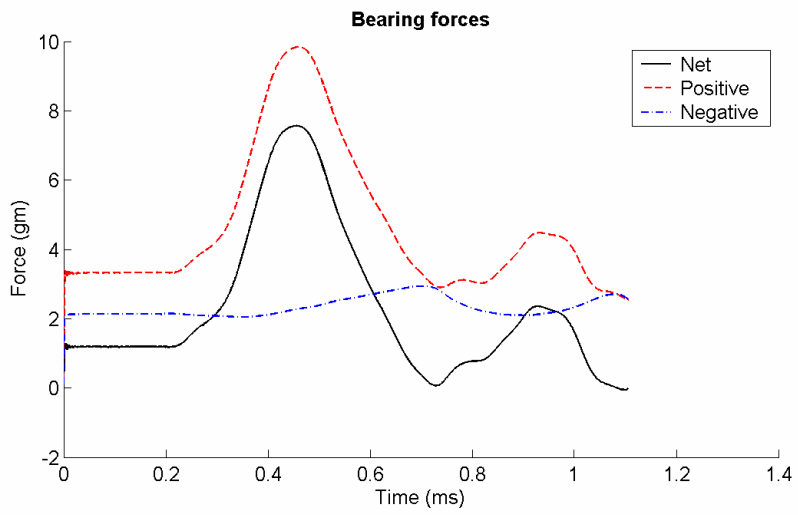


Fig 17. Air bearing and contact forces for negative 800 G shock

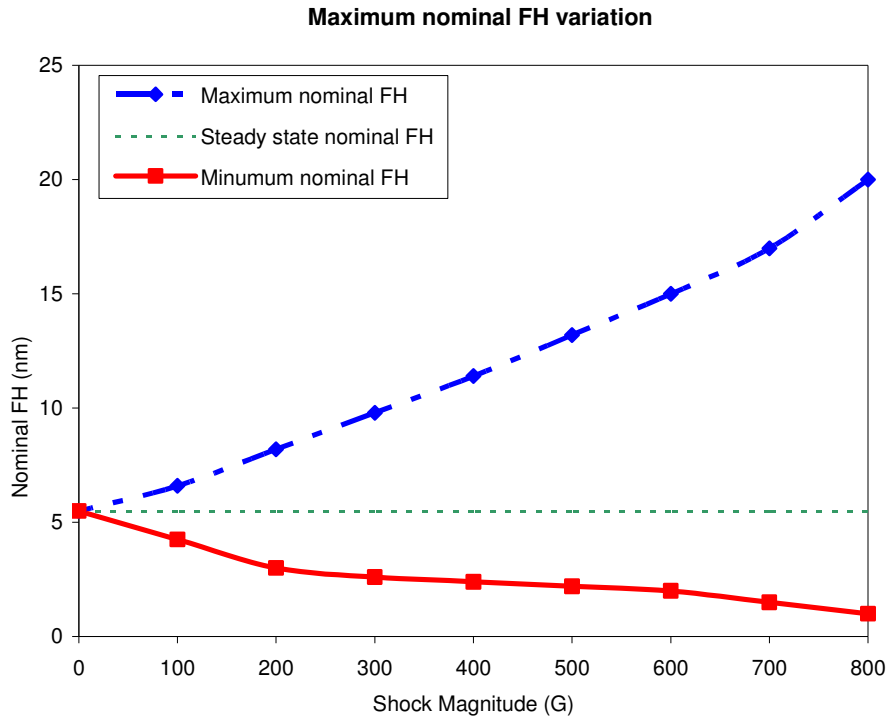


Fig 18. Nominal fly height variation for negative shock

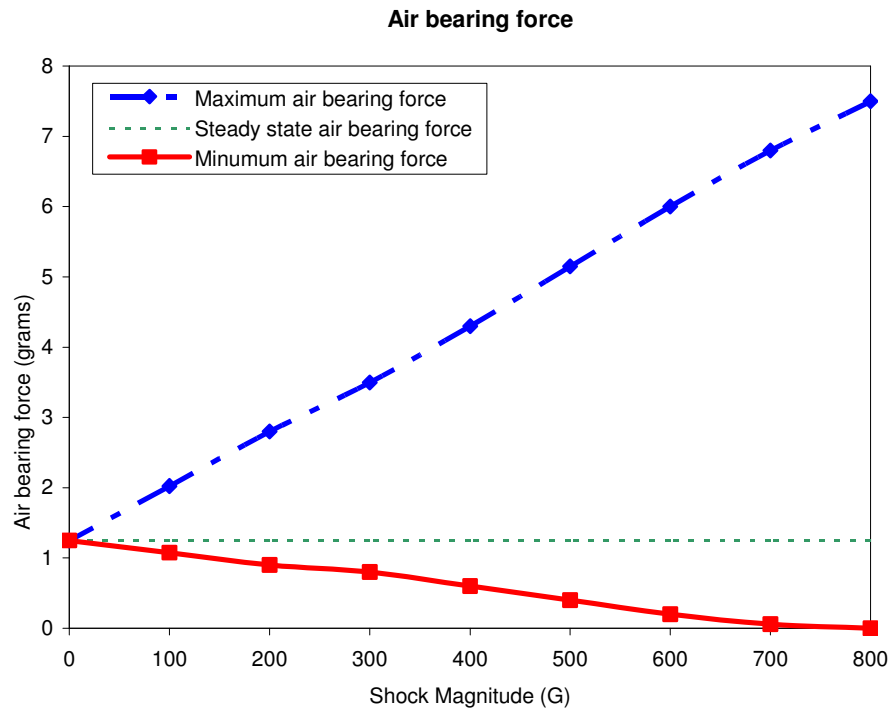


Fig 19. Air bearing force variation for negative shock

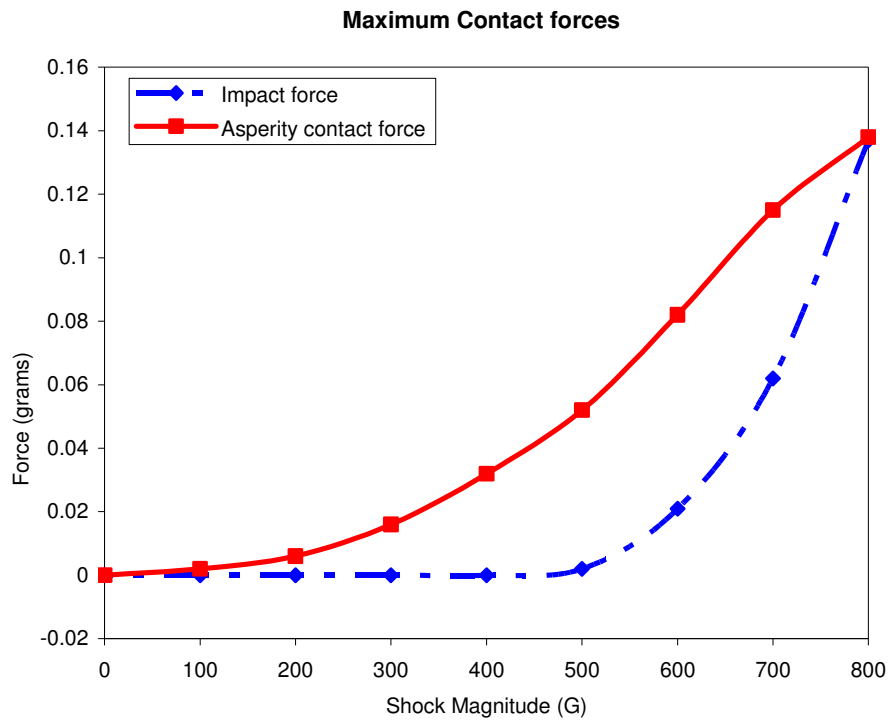


Fig 20. Maximum contact force variation for negative shock

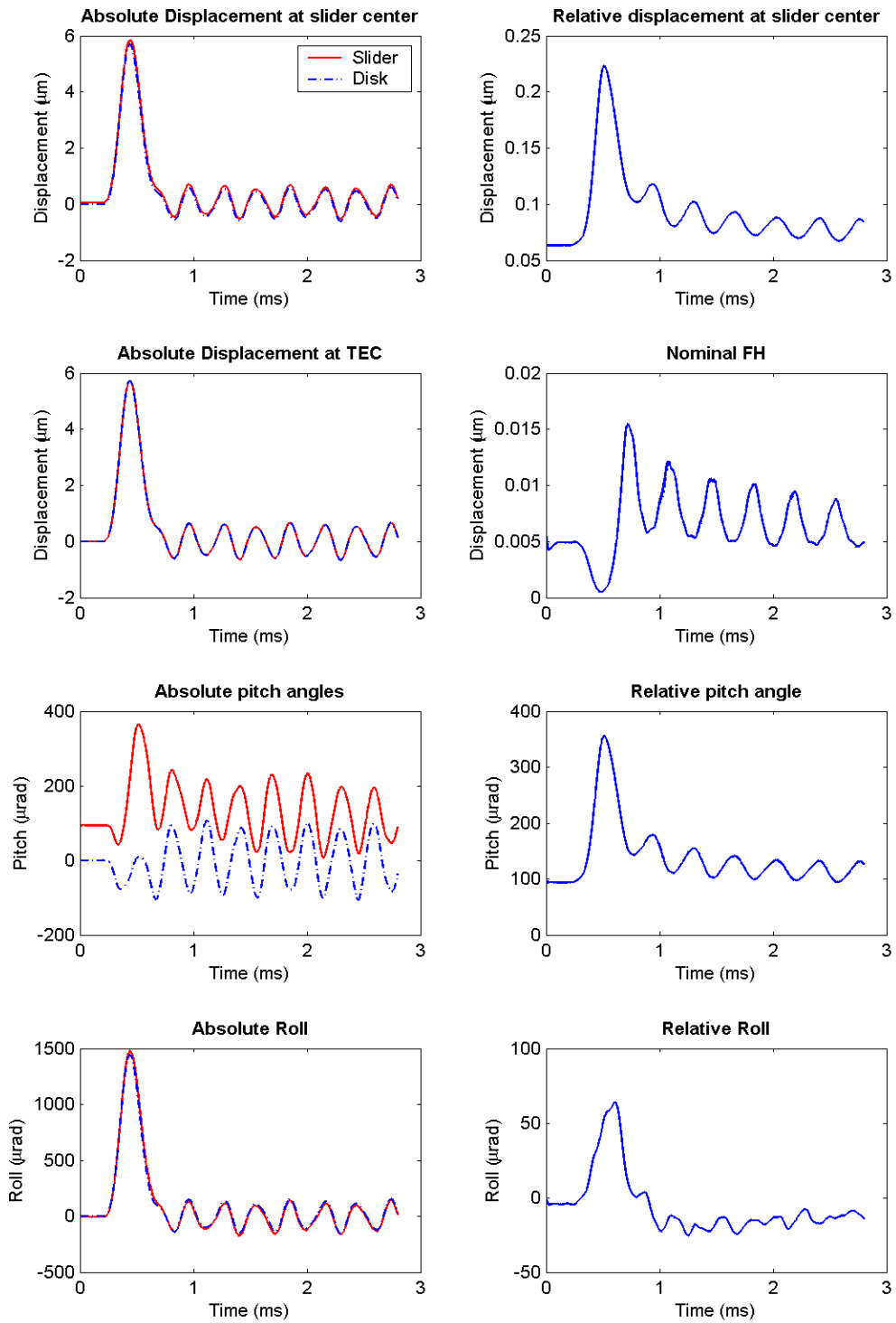


Fig 21. Absolute and relative attitude for positive 200 G shock

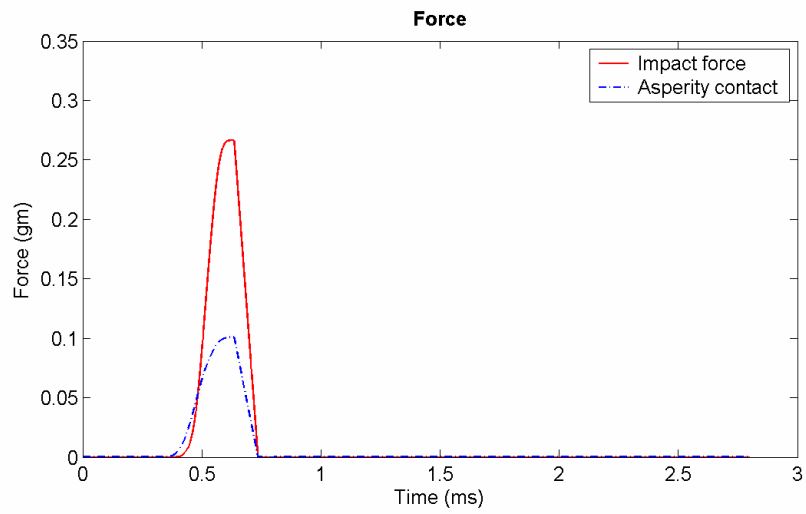
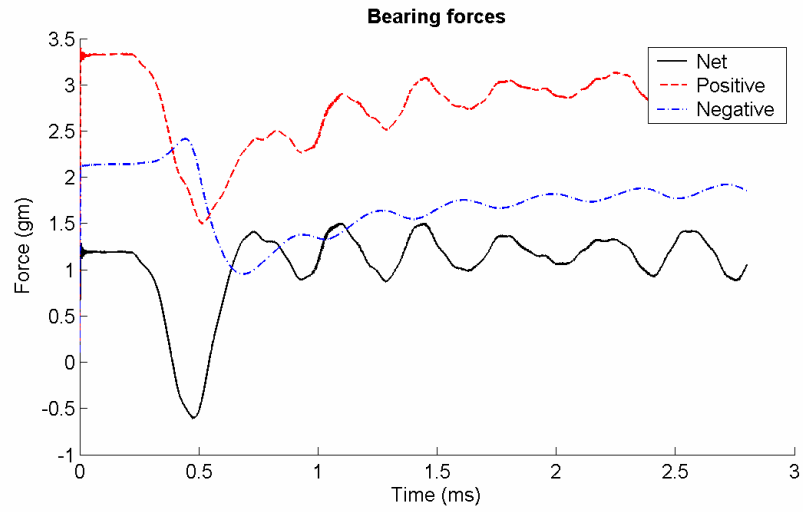


Fig 22. Air bearing and contact forces for positive 200 G shock

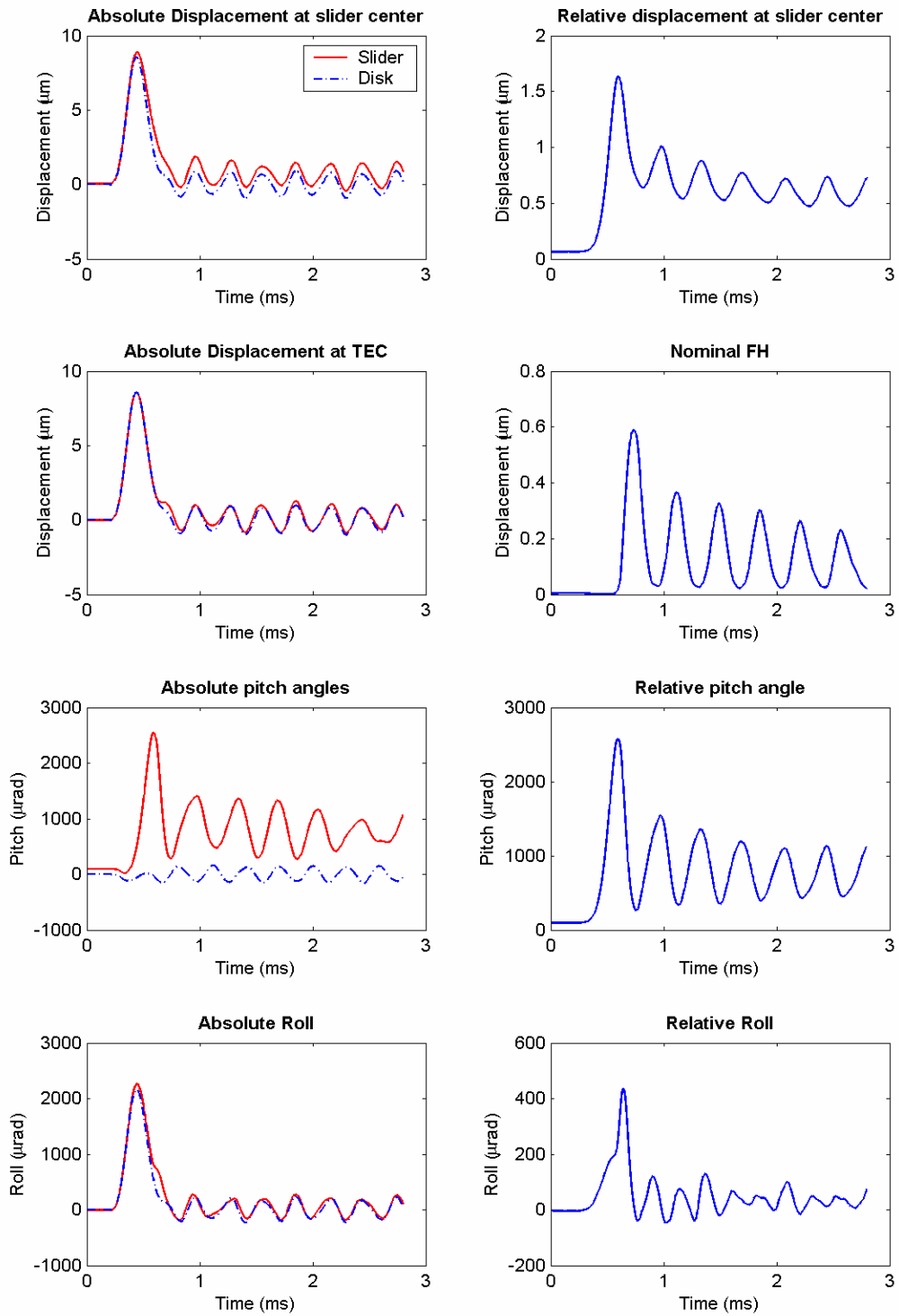


Fig 23. Absolute and relative attitude for positive 300 G shock

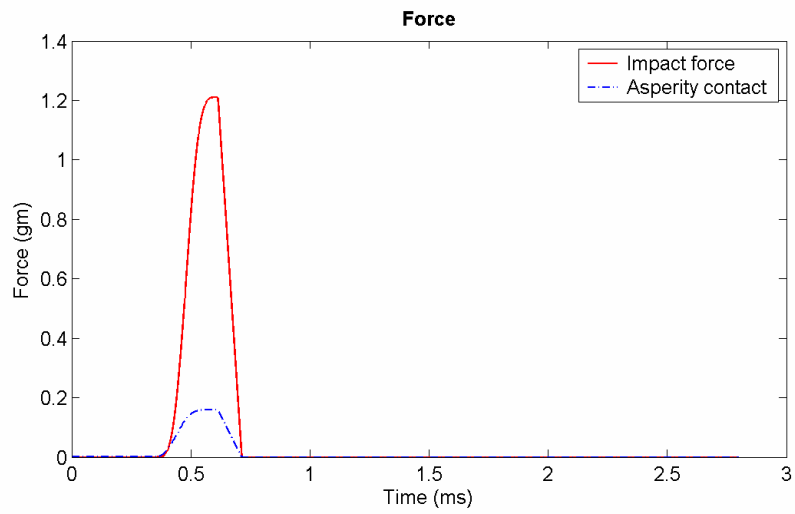
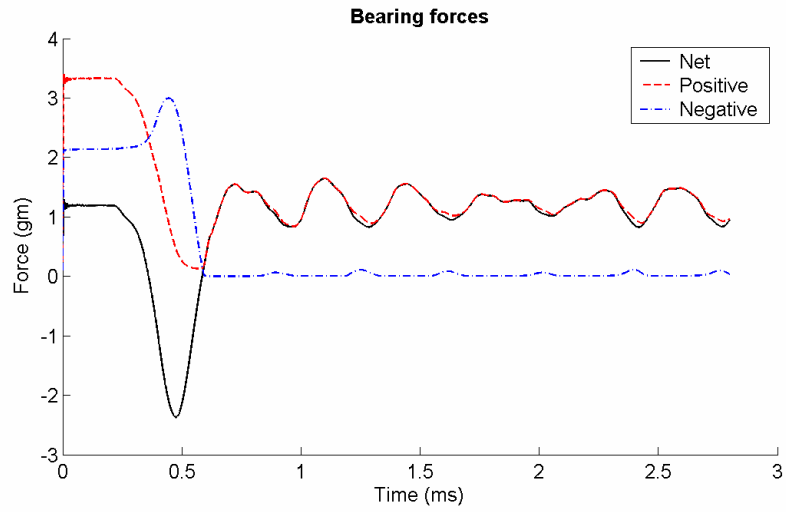


Fig 24. Air bearing and contact forces for positive 300 G shock

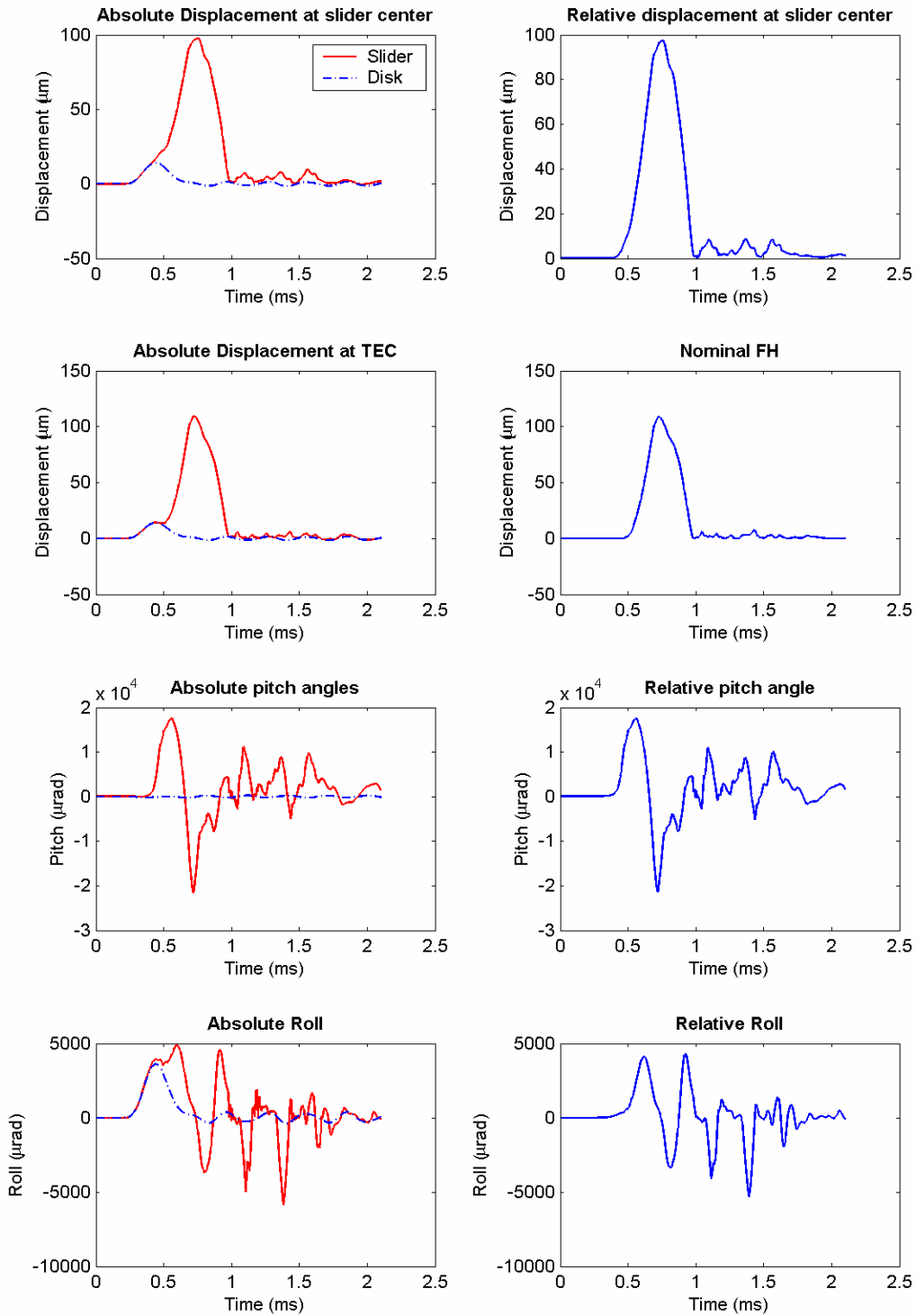


Fig 25. Absolute and relative attitude for positive 500 G shock

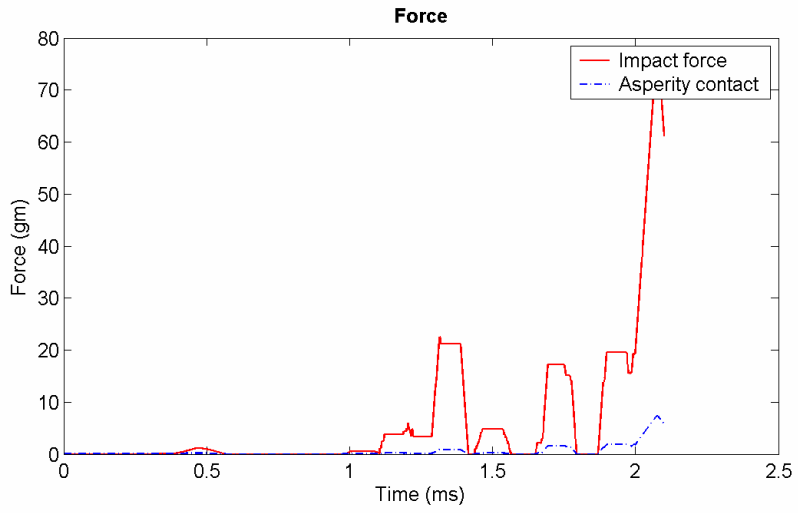
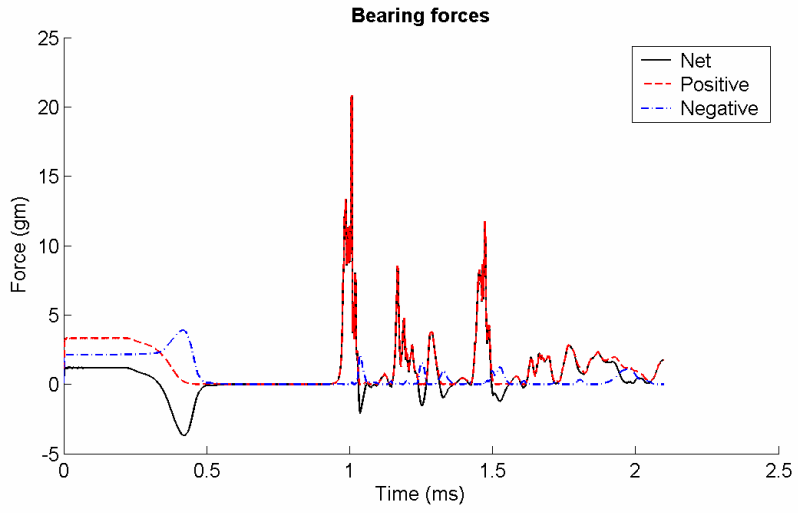


Fig 26. Air bearing and contact forces for positive 500 G shock

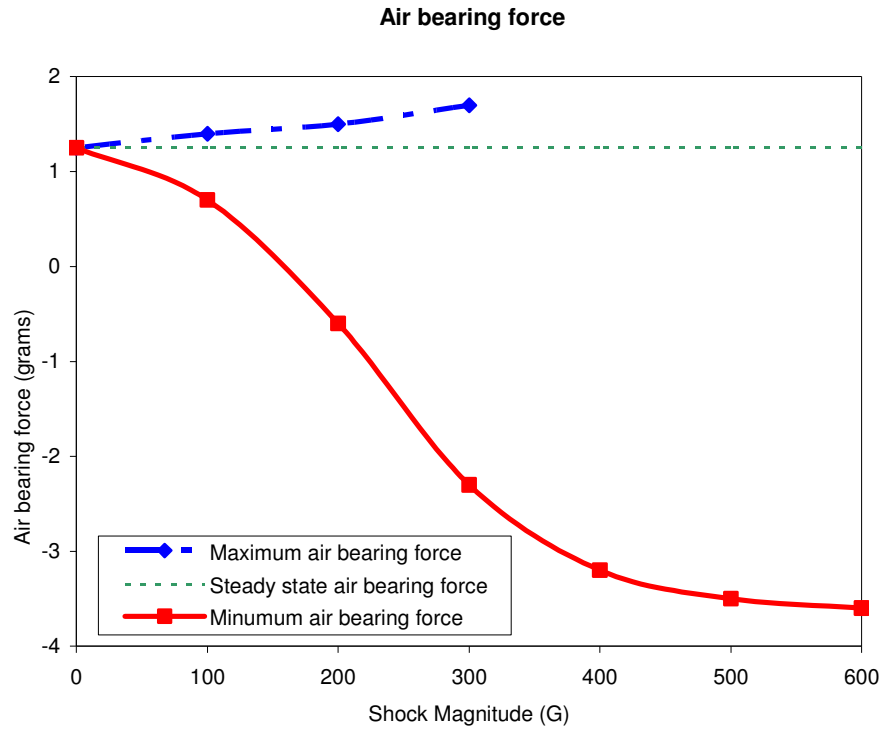


Fig 27. Air bearing force variation for positive shock

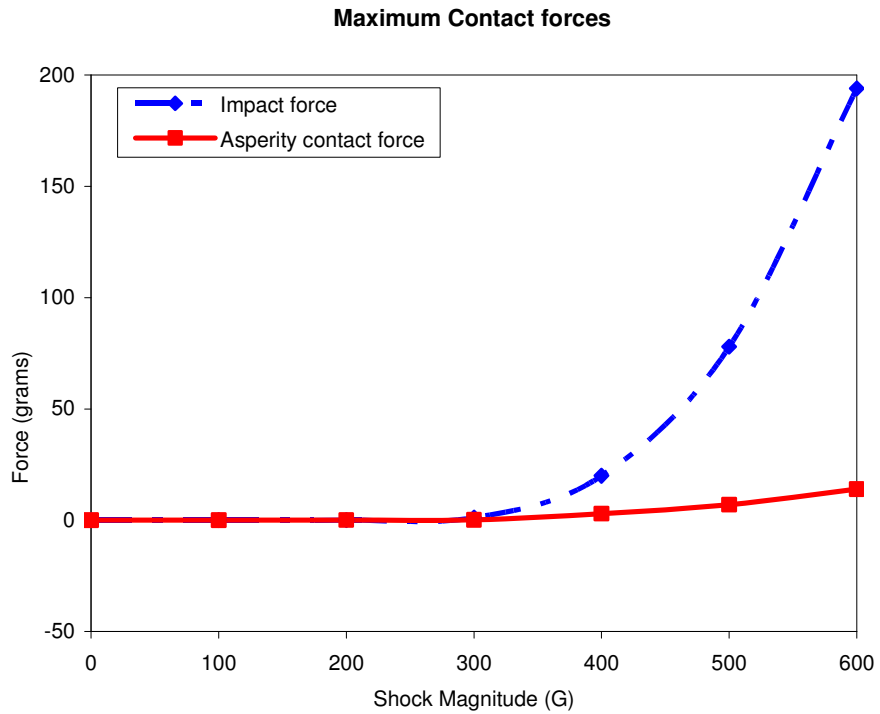


Fig 28. Maximum contact force variation for negative shock